Transactions of the TSME (2018) Vol. 6, No. 2, 95-112
Journal of Research and Applications in Mechanical Engineering

ISSN 2229–2152 print
DOI: 10.14456/jrame.2018.10

Research Article

TURBULENT FLOW BEHAVIORS ON THERMAL ENHANCEMENT IN A CIRCULAR TUBE HEAT EXCHANGER EQUIPPED WITH SINUSOIDAL BAFFLES

P. Promthaisong[1]
S. Suwannapan[2,*]
[1] *Department of Mechanical Engineering, Faculty of Engineering, Mahanakorn University of Technology, 140 Chueamsamphan Road, Nong Chok, Bangkok 10530, Thailand*
[2] *Department of Mechanical Engineering, Faculty of Engineering, Rajamangala University of Technology Isan, Khonkaen Campus, 150 Srichan Road, Muang, Khonkaen 40000, Thailand*

ABSTRACT:
3D numerical computations based on a circular tube heat exchanger with inserted sinusoidal baffles was performed to gain an understanding of its turbulent flow behavior, temperature field and local Nusselt number field which led to an increased heat transfer and thermal enhancement factor. The sinusoidal baffles were inserted at middle of a test tube and behaved as a turbulator. The computations, based on a finite volume method, were performed at Reynolds numbers ranging from 5000 to 20,000. The effect of operating with a PR = 1.0, 2.0, 3.0 and AR = 0.05, 0.10, 0.15, 0.20, 0.25 with sinusoidal baffles was investigated. From the numerical results, the fluid flow was deflected by the sinusoidal baffles and then impinged upon the tube wall. The thermal boundary layer was disrupted and increased the heat transfer along the test tube. Increased AR and decreased PR values led to increased heat transfer and friction factors. The numerical results showed that the sinusoidal baffles yielded higher Nusselt numbers and friction factors than were observed in a plain tube. The heat transfer, friction factor and thermal enhancement factor were greater than the plain tube by approximately 1.7–7.7, 3.6–117 and 1.12–1.9 times, respectively. Operating at PR = 2.0 and AR = 0.20 provided the maximum thermal enhancement factor of 1.9 at Re=5000.

Keywords: *Sinusoidal baffle, Turbulent flow, Nusselt number, Friction factor, Thermal enhancement factor*

1. INTRODUCTION

Baffles inserted into a circular tube heat exchanger have been widely used for enhancing the convective heat transfer coefficient, especially in heat exchangers, to reduce costs, size and installation area. The major purpose for their use is to disrupt the thermal boundary layer along the tube wall. A plain tube shows a thermal boundary layer with increasing thickness. However, various baffle geometries, heights and pitches result in different impacts on the overall thermal performance. Therefore, a baffle geometry which results in high heat transfer and low–pressure drop is the goal of researchers, to increase the overall thermal performance of such heat exchangers.

For decades, baffles of various geometries were inserted in the core of circular tube heat exchangers. The impacts on their Reynold numbers and baffle parameters were studied and the effects upon heat transfer and the friction factor were compared with that of plain tubes. Overall thermal performance is reported in terms of a thermal

* Corresponding author: S. Suwannapan
E–mail address: oak_su@hotmail.com

enhancement factor (*TEF*) at equal pumping power comparing heat transfer and pressure drop with tube inserts and plain tubes. If the *TEF* is higher than 1.0, there is an overall thermal performance gain. Deshmukh and Vedula [1] and Deshmukh et al. [2] presented the effect of a delta wing vortex generator in a circular tube. They concluded that the mainstream fluid was directed towards the tube wall by the delta wing vortex generator leading to increased heat transfer.

Chokphoemphun et al. [3] investigated the enhancement of heat transfer and reduction of pressure loss using single, double, triple, and quadruple twisted–tape inserts in circular tubes. They found that the twisted–tape in all cases provided higher heat transfer than a plain tube due to swirl flow. Chokphoemphun et al. [4] reported the effect of a winglet vortex generator on heat transfer in a circular tube. The results showed that winglet vortex generator produced two counter–rotating vortices along the tube that helped to increase the heat transfer due to increased fluid mixing. Tamna et al. [5] indicated that winglet–pairs generated four counter–rotating vortices along the tube leading to increased flow mixing. Skullong et al. [6–9] reported the effect of various winglet geometries placed on smooth/perforated tapes inserted into circular tubes. They found that the heat transfer was improved over that of a plain tube because of increased fluid mixing at the core and the near-wall region. They found that a perforated winglet/tape reduced the friction factor more than a smooth winglet/tape. Wijayanta et al. [10] studied the effect of a punched delta winglet vortex generator in a circular tube with various attack angles. The results indicated that an increased attack angle led to both increased heat transfer and friction factors. The fluid flow became more turbulent, which helped to increase the disturbance at the thermal boundary layer leading to an increased convective heat transfer coefficient. Chamoli et al. [11] studied the thermal characteristics of turbulent flow through a circular tube fitted with a perforated vortex generator (PVG). They found that the PVG generated streamwise vortices and increased vortex strength resulting in a remarkable increase in flow mixing between the core and the near-wall region. This resulted in increased heat transfer. The effect of delta–winglet and rectangular winglet vortex generators was presented by Lei et al. [12] and Liu et al. [13], respectively. Their results revealed that the delta-winglet and rectangular winglet vortex generators produced two and four counter–rotating vortices, respectively, leading to increased strong flow at the wall surface that helped to increase heat transfer. Hong et al. [14] studied the heat transfer and fluid flow behaviors in a circular tube with modified wire coils (WCs). Their results revealed that the Nusselt number and friction factor were around 1.46–2.49 and 8.36–18.62 times higher, respectively, over a plain tube. The maximum performance evaluation criterion was 1.14 at the lowest Reynold number. Promthaisong et al. [15] studied the v–cone bundles in a circular tube. They found that the Nusselt number and friction factor higher than a plain tube around 1.49–2.0 and 3.95–8.0 times, respectively. The maximum thermal enhancement factor was 1.01 at the lowest Reynold number.

Table 1: Baffle geometries, parameters and results of previous work.

Researcher	Geometry	Parameter	Result
Deshmukh and Vedula [1]	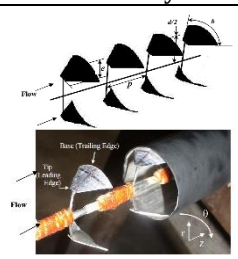	Re = 10,000–45,000 p/pl = 1.4–7.9 e/d = 0.09, 0.17, 0.25 α = 15º ,30º ,45º	Nu_a/Nu_s = 1.3–5.0 Nu_a/Nu_c = 1.0–1.8
Deshmukh et al. [2]	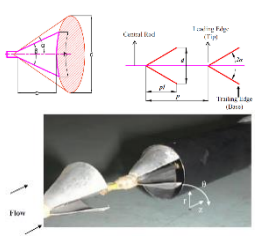	Re = 250–1500 N = 2, 3 p/pl = 1.1–6.2 p/d = 0.6–3.2 b/d = 0.7, 1, 1.3 α = 15º, 30º, 45º, 60º, 75º	Nu_a/Nu_s = 5.0–15.0 Nu_a/Nu_c = 1.0–6.0

Table 1: Baffle geometries, parameters and results of previous work (Cont.).

Researcher	Geometry	Parameter	Result
Chokphoemphun et al. [3]	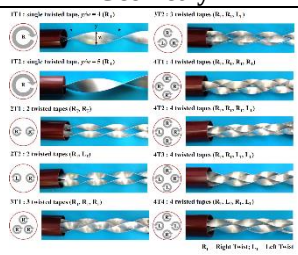	Re = 5300–24,000 y/w = 4, 5	Nu/Nu_0 = 1.15–2.12 f/f_0 = 1.98–4.06 TEF = 0.92–1.33
Chokphoemphun et al. [4]	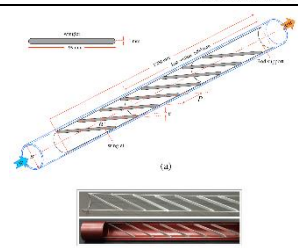	Re = 5300–24,000 P/D = 0.5, 1, 1.5, 2 e/D = 0.1, 0.15, 0.2 α = 30º	Nu/Nu_0 = 2.03–2.34 f/f_0 = 2.07–5.63 TEF = 1.35–1.59
Tamna et al. [5]	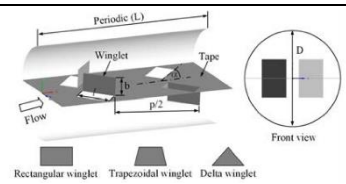	Re = 4000–20,000 b/D = 0.1, 0.15, 0.2, 0.25 p/D = 4 α = 45º	Nu/Nu_0 = 1.8–2.7 f/f_0 = 4.5–11.0 TEF = 1.00–1.48
Skullong et al. [6]	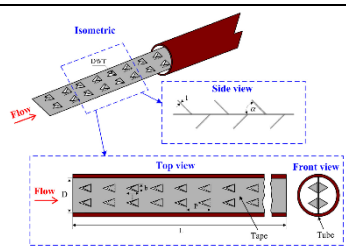	Re = 4200–25,500 P/D = 0.5, 1.0, 1.5, 2.0, 2.5 b/D = 0.2 l/D = 0.4 α = 30º ,45º,60º	Nu/Nu_0 = 2.4–5.1 f/f_0 = 7.5–79.1 TEF = 1.04–1.49
Skullong et al. [7]	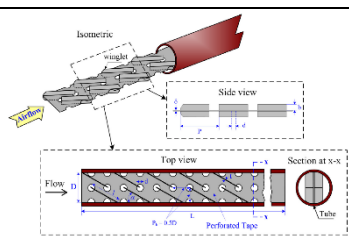	Re = 4180–26,000 P_R = 0.5, 1.0, 1.5 B_R = 0.1, 0.15, 0.2, 0.25, 0.3 α = 30º	Nu/Nu_0 = 2.4–4.77 f/f_0 = 5.0–42.9 TEF = 1.34–1.71
Skullong et al. [8]	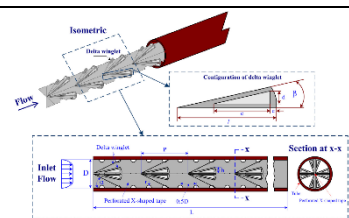	Re = 4180–26,000 P_R = 0.5, 1.0, 1.5, 2.0 B_R = 0.1, 0.15, 0.2, 0.25 A_p/A_w = 0.359 α = 30º	Nu/Nu_0 = 2.0–5.06 f/f_0 = 2.06–35.68 TEF = 1.42–1.9
Skullong et al. [9]	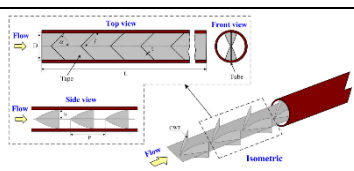	Re = 4150–25,400 P_R = 0.5, 1.0, 2.0 B_R = 0.1, 0.2, 0.3 α = 45º	Nu/Nu_0 = 3.4–4.8 f/f_0 = 2.06–35.68 TEF = 1.22–1.75

Table 1: Baffle geometries, parameters and results of previous work (Cont.).

Researcher	Geometry	Parameter	Result
Wijayanta et al. [10]	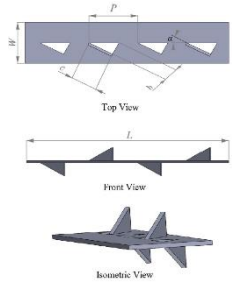	Re = 5500–14,500 R_P = 1.05 R_B = 0.42 α = 30º ,50º,70º	Nu = 40–330 f = 0.1–0.51 TEF = 0.88–1.22
Chamoli et al. [11]	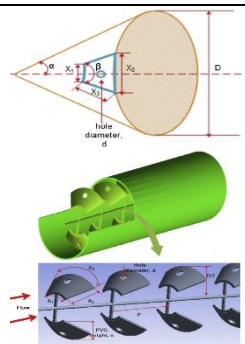	Re = 3000–21,000 PI = 4%, 8%, 12%, 16% p/p_a = 2, 4, 6 e/D = 0.25 α = 45º	Nu/Nu_0 = 2.11–4.04 f/f_0 = 4.12–22.53 TEF = 1.13–1.65
Lei et al. [12]	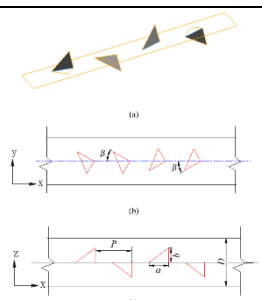	Re = 6000–20,000 P = 1D, 2D, 3D, 4D β = 15º ,30º ,45º,60º	Effcet of β; Nu = 50–250 f = 0.03–0.21 Effcet of P; Nu = 50–220 f = 0.03–0.13 TEF = 1.06–1.35
Liu et al. [13]	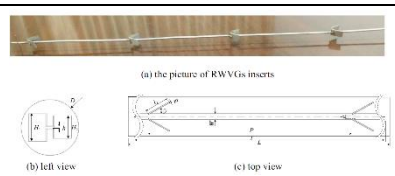	Re = 5000–17,000 $H1/D$ = 0.5 $H2/D$ = 0.2, 0.3, 0.4, 0.5 β = 10º ,20º ,30º,35º	Nu/Nu_0 = 1.16–2.49 f/f_0 = 2.09–12.32 TEF = 0.82–1.18
Hong et al. [14]	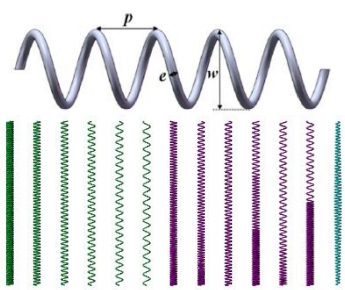	Re = 6000–20,000 WCs–UP; p/d = 0.172–1.034 WCs–VP; p/d = 0.172–0.690 WCs–GVW; w/d = 0.552–0.897–0.552	Nu/Nu_0: WCs–UP = 1.46–2.49 WCs–VP = 1.75–2.30 WCs–GVW = 2.2–2.31 f/f_0; WCs–UP = 8.36–17.82 WCs–VP = 0.49–18.33 WCs–GVW = 15.99–18.62 TEF = 0.69–1.14
Promthaisong et al. [15]	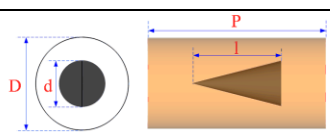	Re = 5000–15,000 P/D = 1.0, 2.0, 3.0, 4.0 d/D = 0.5	Nu/Nu_0 = 1.49–2.0 f/f_0 = 3.95–8.0 TEF = 0.92–1.01

The baffle geometries, parameters and results of previously published studies are displayed in Table. 1. All of these studies found that heat transfer was increased by using inserted baffles in circular tubes. However, the friction factor also increased due to increased resistance to flow. At the same pumping power used in plain tubes, it can be clearly seen that most baffled tubes exhibited *TEF* values that were greater than 1.0, depending on baffle geometry and other parameters. This indicated an overall improvement in thermal performance. In the current study, the effects upon thermal performance using a novel sinusoidal baffle inserted into a circular tube was investigated. The flow structure and heat transfer behavior were investigated. To achieve the maximum thermal enhancement factor, the effect of varying *AR* (0.05, 0.10, 0.15, 0.20, 0.25) and *PR* (1.0, 2.0, 3.0) values was investigated in turbulent flow regimes ranging from *Re* 5000 to 20,000. A comparison of the maximum thermal enhancement factors from the literature with that of a tube containing a sinusoidal baffle is reported.

2. TUBE GEOMETRY AND BOUNDARY CONDITIONS

The geometry of a circular tube heat exchanger equipped with a sinusoidal baffle and the computational domain of the periodic module are presented in Fig. 1. The tube diameter, *D*, was 0.05 m. The sinusoidal baffle pitch, *p*, was varied in terms of its pitch ratio, *p/D*, as *PR* = 1.0, 2.0 and 3.0. The sinusoidal baffle amplitude, e, was varied in terms of its amplitude ratio, *e/D*, *AR* = 0.05, 0.10, 0.15, 0.20 and 0.25 in a turbulent regime, *Re* = 5000–20,000. The entire length of a circular tube heat exchanger equipped with sinusoidal baffles was used to investigate the fully developed periodic flow and heat transfer. The computational domain was divided into three sections, entry, heating and exit sections. The entry, heating and exit lengths were 10*D*, 15*D* and 5*D*, respectively, as is shown in Fig. 2. High density grid hexahedron cells were generated in the near-wall region since the first layer is next to the tube wall in the computational domain. The intensity of turbulent flow can significantly change in the momentum and heat transfers equations. To resolve this problem, an Enhanced Wall Treatment (EWT) near–wall equation was used for the *k–ε* equation with the realizable *k–ε* turbulent model. In the present work, the boundary conditions can be summarized as follows:

- The computational domain of the periodic module tube equipped with sinusoidal baffles was set equal to the periodic conditions at the inlet and outlet.
- The inlet and outlet conditions were set, specifying the inlet velocity and outlet pressure conditions.
- The tube walls and sinusoidal baffles had a no–slip condition.
- The tube wall had a constant heat flux of 600 w/m^2.
- The sinusoidal baffles were assumed to be insulators.
- Air (Pr = 0.707) was used as the working fluid at 300 K and its physical properties were assumed to remain constant at the average bulk mean temperature.

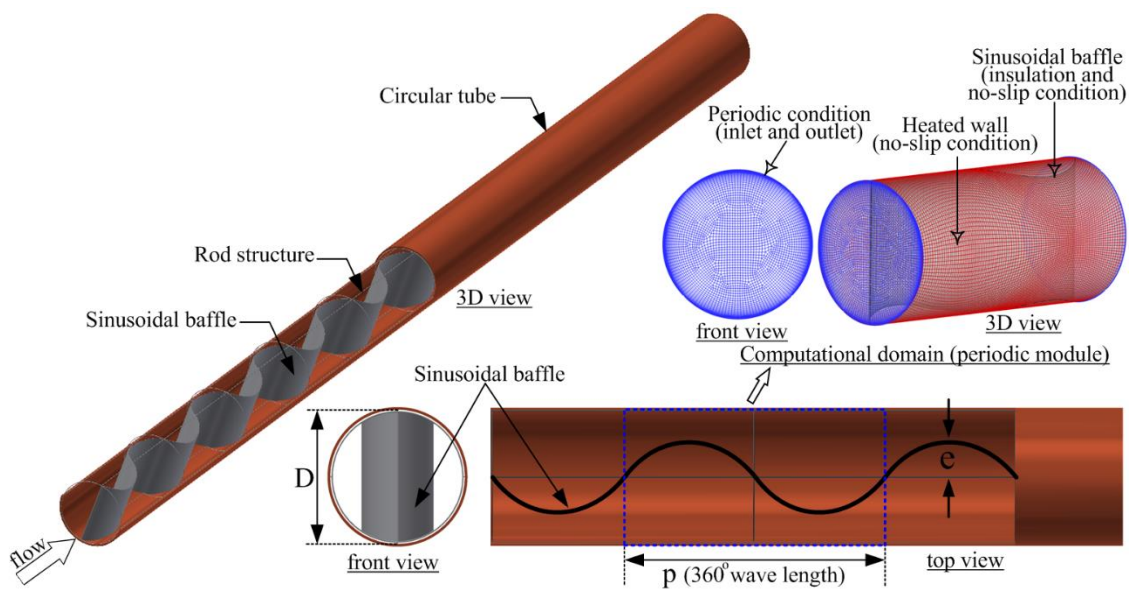

Fig. 1. The geometry of the circular tube heat exchanger equipped with sinusoidal baffles and computational domain of the periodic module.

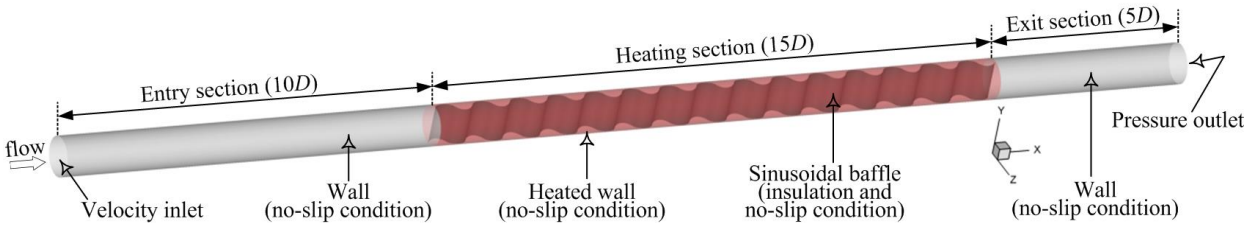

Fig. 2. Computational domain and boundary conditions of the full length.

3. THE ASSUMPTIONS, MATHEMATICAL FOUNDATION AND PARAMETERS OF INTEREST

The assumptions for the flow and heat transfer problems in the present work are steady state three–dimensional, turbulent and incompressible flow. Convective heat transfer was considered while natural convection, body forces, viscous dissipation and radiation heat transfer were disregarded. The flow and heat transfer were governed by the continuity, Navier–Stokes and energy equations. The Quadratic Interpolation for Convective Kinetics scheme (QUICK) was applied to all equations. The SIMPLE algorithm and finite volume approach [16] were used to solve the flow and heat transfer problems. The normalized residual values were considered convergent when the residuals of the energy and other equations were less than 10^{-9} and 10^{-5}, respectively. The governing equations in the Cartesian tensor system can be written as:

Continuity equation:

$$\frac{\partial(\rho u_{\mathrm{i}})}{\partial x_{\mathrm{i}}} = 0 \tag{1}$$

Momentum equation:

$$\frac{\partial(\rho u_{\mathrm{i}} u_{\mathrm{j}})}{\partial x_{\mathrm{j}}} = -\frac{\partial P}{\partial x_{\mathrm{i}}} + \frac{\partial}{\partial x_{\mathrm{j}}}\left[\mu\left(\frac{\partial u_{\mathrm{i}}}{\partial x_{\mathrm{j}}} + \frac{\partial u_{\mathrm{j}}}{\partial x_{\mathrm{i}}} - \frac{2}{3}\delta_{\mathrm{ij}}\frac{\partial u_{\mathrm{l}}}{\partial x_{\mathrm{l}}}\right)\right] + \frac{\partial}{\partial x_{\mathrm{j}}}\left(-\rho\overline{u_{\mathrm{i}}' u_{\mathrm{j}}'}\right) \tag{2}$$

where $u_i = \bar{u}_{\mathrm{i}} + u_{\mathrm{i}}'$ and $-\rho\overline{u_i' u_{\mathrm{j}}'}$ are the Reynolds stresses, displayed as:

$$-\rho\overline{u_{\mathrm{i}}' u_{\mathrm{j}}'} = \mu_{\mathrm{t}}\left(\frac{\partial u_{\mathrm{i}}}{\partial x_{\mathrm{j}}} + \frac{\partial u_{\mathrm{j}}}{\partial x_{\mathrm{i}}}\right) - \frac{2}{3}\left(\rho k + \mu_{\mathrm{t}}\frac{\partial u_{\mathrm{k}}}{\partial x_{\mathrm{k}}}\right)\delta_{\mathrm{ij}} \tag{3}$$

where k is the turbulent kinetic energy, $k = 0.5\overline{u_{\mathrm{i}}' u_{\mathrm{j}}'}$ and $\mu_{\mathrm{t}} = \rho c_{\mu} k^2 / \varepsilon$.

Energy equation:

$$\frac{\partial}{\partial x_{\mathrm{i}}}\left[u_{\mathrm{i}}(\rho E + P)\right] = \frac{\partial}{\partial x_{\mathrm{j}}}\left[\left(k + \frac{c_{\mathrm{p}}\mu_{\mathrm{t}}}{\mathrm{Pr}_{\mathrm{t}}}\right)\frac{\partial T}{\partial x_{\mathrm{j}}} + u_{\mathrm{i}}\left(\tau_{\mathrm{ij}}\right)_{\mathrm{eff}}\right] \tag{4}$$

where E is the total energy and $\left(\tau_{\mathrm{ij}}\right)_{\mathrm{eff}}$ is the deviatoric stress tensor, defined as:

$$\left(\tau_{\mathrm{ij}}\right)_{\mathrm{eff}} = \mu_{\mathrm{eff}}\left(\frac{\partial u_{\mathrm{j}}}{\partial x_{\mathrm{i}}} + \frac{\partial u_{\mathrm{i}}}{\partial x_{\mathrm{j}}}\right) - \frac{2}{3}\mu_{\mathrm{eff}}\frac{\partial u_{\mathrm{k}}}{\partial x_{\mathrm{k}}}\delta_{\mathrm{ij}} \tag{5}$$

The realizable k-ε turbulent model was used in the present work and the modeled transport equations for k and ε can be expressed as:

$$\frac{\partial\left(\rho k u_{\mathrm{j}}\right)}{\partial x_{\mathrm{j}}}=\frac{\partial}{\partial x_{\mathrm{j}}}\left[\left(\mu+\frac{\mu_{\mathrm{t}}}{\sigma_{\mathrm{k}}}\right)\frac{\partial k}{\partial x_{\mathrm{j}}}\right]+G_{\mathrm{k}}+G_{\mathrm{b}}-\rho\varepsilon+S_{\mathrm{k}} \tag{6}$$

and

$$\frac{\partial\left(\rho\varepsilon\ u_{\mathrm{j}}\right)}{\partial x_{\mathrm{j}}}=\frac{\partial}{\partial x_{\mathrm{j}}}\left[\left(\mu+\frac{\mu_{\mathrm{t}}}{\sigma_{\varepsilon}}\right)\frac{\partial\varepsilon}{\partial x_{\mathrm{j}}}\right]+\rho C_1 S\varepsilon-\rho C_2\frac{\varepsilon^2}{k+\sqrt{\nu\varepsilon}}+C_{1\varepsilon}\frac{\varepsilon}{k}C_{3\varepsilon}G_{\mathrm{b}}+S_{\varepsilon} \tag{7}$$

where

$$C_1=\max\left[0.43,\frac{\eta}{\eta+5}\right],\ \eta=Sk/\varepsilon,\ S=\left(2S_{\mathrm{ij}}S_{\mathrm{ij}}\right)^{0.5},\ S_{\mathrm{ij}}=0.5\left(\frac{\partial u_{\mathrm{j}}}{\partial x_{\mathrm{i}}}+\frac{\partial u_{\mathrm{i}}}{\partial x_{\mathrm{j}}}\right) \tag{8}$$

the realizable k-ε turbulent model constants are given as follows:

$$\sigma_{\mathrm{k}}=1.0,\ \sigma_{\varepsilon}=1.2,\ C_{1\varepsilon}=1.44,\ C_2=1.9 \tag{9}$$

Dimensionless parameters were used in the present work to investigate heat transfer and the pressure drop. The air velocity is presented in terms of the Reynolds number, *Re*, at the tube inlet.

$$\mathrm{Re}=UD_{\mathrm{h}}/\nu \tag{10}$$

The pressure drop across the test section is presented in the form of the friction factor (f) and friction factor ratio (f/f_0). The friction factor can be calculated from the pressure gradient across a periodic module as:

$$f=\left(-dP/dx\right)\cdot D_{\mathrm{h}}\Big/\frac{1}{2}\rho U^2 \tag{11}$$

where U is the mean air velocity and D_{h} is the hydraulic diameter of the tube which can be seen in the Ref. [17].

The heat transfer rate was reported in terms of the average Nusselt number (Nu) and Nusselt number ratio (Nu/Nu_0). The average Nusselt number of a circular tube equipped with sinusoidal baffles can be obtained using the local Nusselt number, Nu_{x}, which is calculated as:

$$\mathrm{Nu}_{\mathrm{x}}=h_{\mathrm{x}}D_{\mathrm{h}}/k_{\mathrm{a}} \tag{12}$$

and

$$\mathrm{Nu}=\frac{1}{A}\int Nu_{\mathrm{x}}dA \tag{13}$$

where h_{x} and k_{a} are the convective heat transfer coefficient and the thermal conductivity of air, respectively. The parameter, A, is the area available for heat transfer.

The overall thermal performance of the circular tube equipped with sinusoidal baffles is presented in terms of the thermal enhancement factor (*TEF*). The *TEF* is calculated as the ratio of the heat transfer coefficient of the tube equipped with sinusoidal baffles, h, compared to that of a plain tube, h_0, at an equal pumping power. *TEF* values greater than 1.0 indicate an overall energy gain.

$$\mathrm{TEF} = \left.\frac{h}{h_0}\right|_{\mathrm{pp}} = \left.\frac{\mathrm{Nu}}{\mathrm{Nu}_0}\right|_{\mathrm{pp}} = \left(\frac{\mathrm{Nu}}{\mathrm{Nu}_0}\right)\left(\frac{f}{f_0}\right)^{-1/3} \tag{14}$$

where h_0, Nu_0 and f_0 are heat transfer coefficients, Nusselt number and friction factor of a plain tube, respectively.

4. Results and Discussion

4.1 Verification of parameters of plain tubes

The reliability of the numerical results for the flow and heat transfer in circular tubes equipped with sinusoidal baffles was validated in three ways, verification of the plain tube, verification of the circular tube equipped with the baffles and grid independence.

Figure 3 details the verification of the plain tube. The numerical effects using the standard k–ε, Realizable k–ε and SST k–ω turbulent models on the Nusselt number and friction factor are compared with the correlations of Dittus-Boelter and Blasius [18], as depicted in Eqs. (15–16) and experimental data [19].

Dittus–Boelter correlation:

$$\mathrm{Nu} = 0.023\mathrm{Re}^{0.8}\mathrm{Pr}^{0.4} \tag{15}$$

Blasius correlation:

$$f = 0.316\ \mathrm{Re}^{-0.25} \tag{16}$$

The average Nusselt number and friction factor in the Realizable k–ε turbulent model showed minimal deviations from the correlations of 7.5% and 5.2%, respectively, and from the experimental data of 8.1% and 6.2%, respectively, under similar conditions. Therefore, in computations modelling a circular tube equipped with sinusoidal baffles, the Realizable k–ε turbulent model was used.

Many researchers have used the Realizable k–ε turbulent model to resolve turbulent flow and heat transfer problems in circular tubes equipped with baffles [20–22]. They concluded that the Realizable k–ε turbulent model provided Nusselt numbers and friction factors that were close to experimentally derived data. This indicated that the Realizable k–ε turbulent model can be applied with reattachment and separated flow behavior caused by baffles.

In is necessary to find the optimum number of nodes to reduce computational efforts while retaining high accuracy. The Nusselt number and friction factor were compared using six different grids with 82416, 165248, 326494, 505762, 706425 and 902542 nodes in a computational domain modelling a circular tube equipped with sinusoidal baffles at AR = 0.15, PR = 2.0. The results indicated that three grids with 505762, 706425 and 902542 nodes, gave nearly the same results for all Re. Therefore, the coarsest grid with 505762 nodes was used in the present work.

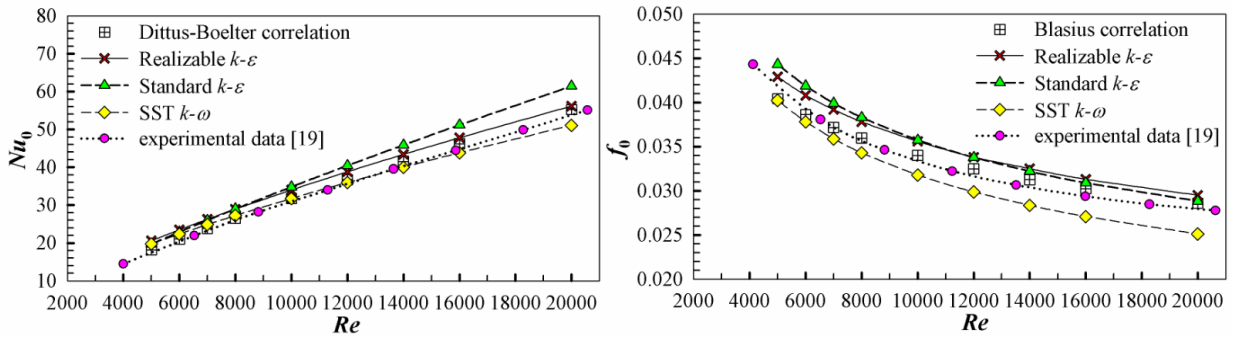

Fig. 3. Verification of Nu_0 and f_0 for a plain tube.

4.2 Fully developed periodic condition

To investigate fully developed periodic on flow and heat transfer, circular tubes equipped with sinusoidal baffles at AR=0.15, PR=1.0 and Re=10,000 were used in the experiments. The heat transfer results with fully developed periodic flow were developed in terms of the three dimensionless parameters of interest, the velocity ratio (u/u_0) and Nusselt number ratio (Nu/Nu_0) profiles.

Figure 4 depicts the relationship between the u/u_0 profile and x/D using u/u_0 values from y/D = 0.5 and z/D = 0.4. The velocity contour and isosurface are displayed to indicate the velocity behavior. In general, u/u_0 increased at the entry of the heating section, and then, the u/u_0 exhibits sine wave behavior due to variation in the cross–sectional area available for flow. In the figure, the u/u_0 profile is divided into two sections, developing and fully developed periodic profiles. The developing flow appears at x/D = 0–8 (8D lengths from the entry section). In this section, the u/u_0 profile does not have similar patterns, especially, for the u/u_0 values. A changing velocity contour and isosurface can be clearly seen as a result of the developing flow. After that, the flow velocity became fully developed and periodic, beginning at x/D = 8. In this section, both the patterns and u/u_0 values for each module were similar. The velocity contour and isosurface for each module are also similar.

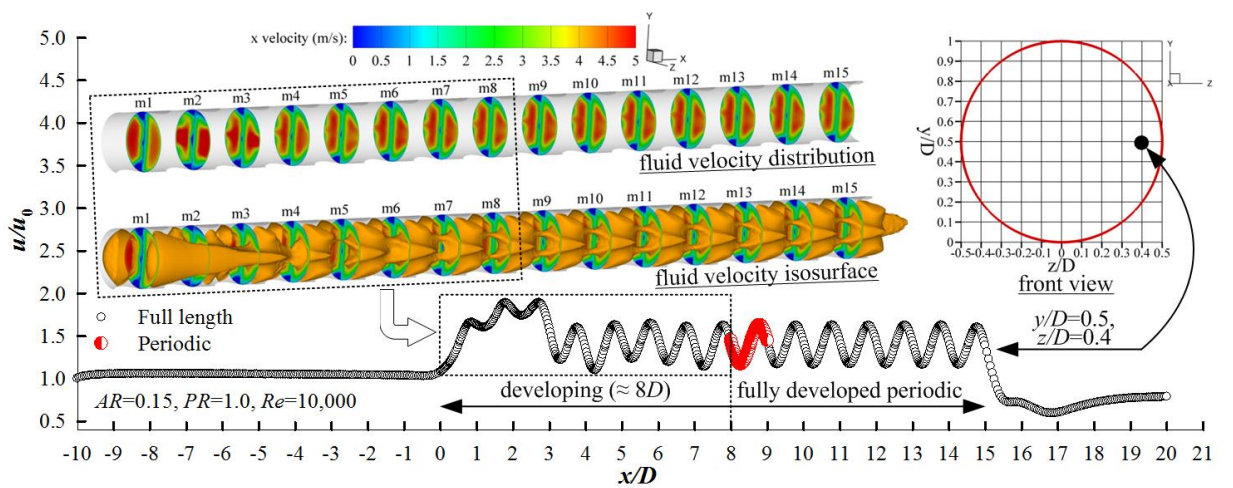

Fig. 4. Fully developed periodic flow.

Fully developed periodic heat transfer is depicted in Fig. 5. The Nu/Nu_0 at the heating section surface at y/D = 1.0 and z/D = 0 was used to indicate the x/D. The local wall Nusselt number contour (Nu) is also displayed. In the figure, it can be clearly seen that the circular tube equipped with sinusoidal baffles appeared to develop improved heat transfer at x/D = 0–7, where both the heat transfer and flow patterns at each module were dissimilar. Then, the heat transfer became fully developed and periodic at about 7D from the heating section. After this, the heat transfer characteristics of each module were similar.

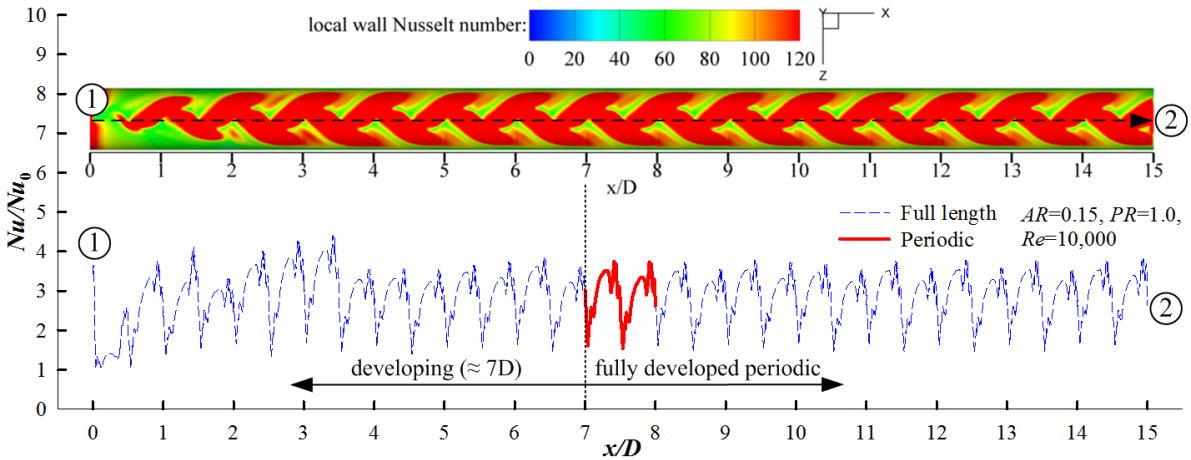

Fig. 5. Fully developed periodic heat transfer.

Both the pattern and values at the inlet and outlet of each module show that velocity and heat transfer in the fully developed periodic region were similar. Therefore, since the tube heat exchanger is very long, the periodic condition can be applied at both the inlet and outlet of the periodic module leading to a reduced number nodes in the grid, reducing computational effort while retaining precision.

4.3 Flow behavior and turbulent kinetic energy distribution

Figure 6 compares the 3D–flow structure for a plain tube and a circular tube equipped with sinusoidal baffles at *AR*=0.15, *PR*=1.0 at *Re*=5000. The use of sinusoidal baffles resulted in a reattachment of flow at the tube wall while this was not seen in the plain tube (it exhibited only laminar flow). In the figure, the fluid flow impacted at the middle of individual sinusoidal baffles, and then separated to impinge upon the tube wall. This behavior occurred in all modules of the test tube in the regions with fully developed periodic flow. The main effect of this was disruption of the thermal boundary layer, leading to increased heat transfer between the fluid and the tube wall. However, the strong flow pattern in the circular tube equipped with sinusoidal baffles significantly affected heat transfer. This is reflected in the turbulent kinetic energy (*TKE*).

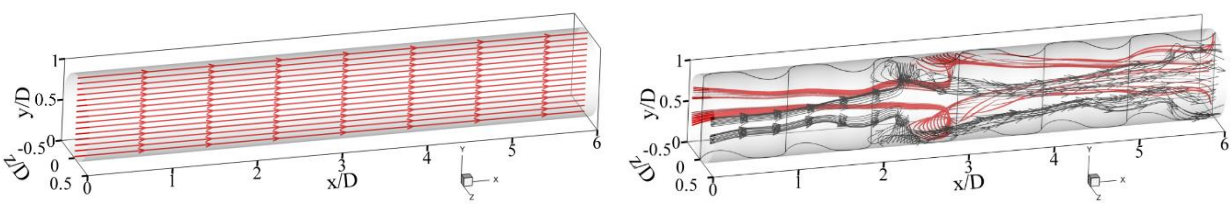

(a) Plain tube (b) *AR*=0.15, *PR*=1.0

Fig. 6. 3D–flow structure at *Re* = 5000.

Figure 7 presents strong flow in terms of the *TKE* distribution in the cross–sectional plane. The flow pattern in the plain tube is displayed as a comparison with a tube equipped with sinusoidal baffles. The effect of *AR* and *PR* are depicted at *Re* = 5000. In general, the tube equipped with sinusoidal baffles had increased *TKE*. Increasing AR resulted in increased *TKE* due to the smaller area available for flow leading to acceleration of the fluid, especially at *AR* = 0.25. Sinusoidal baffles can increase the *TKE* near the tube wall and help to disrupt the thermal boundary layer near the wall. Alternatively, an increased *PR* led to decreased *TKE* because the sinusoidal baffles were flattened, especially at small *AR* and high *PR* values. This was ineffective in both accelerating the flow and disrupting the thermal boundary layer.

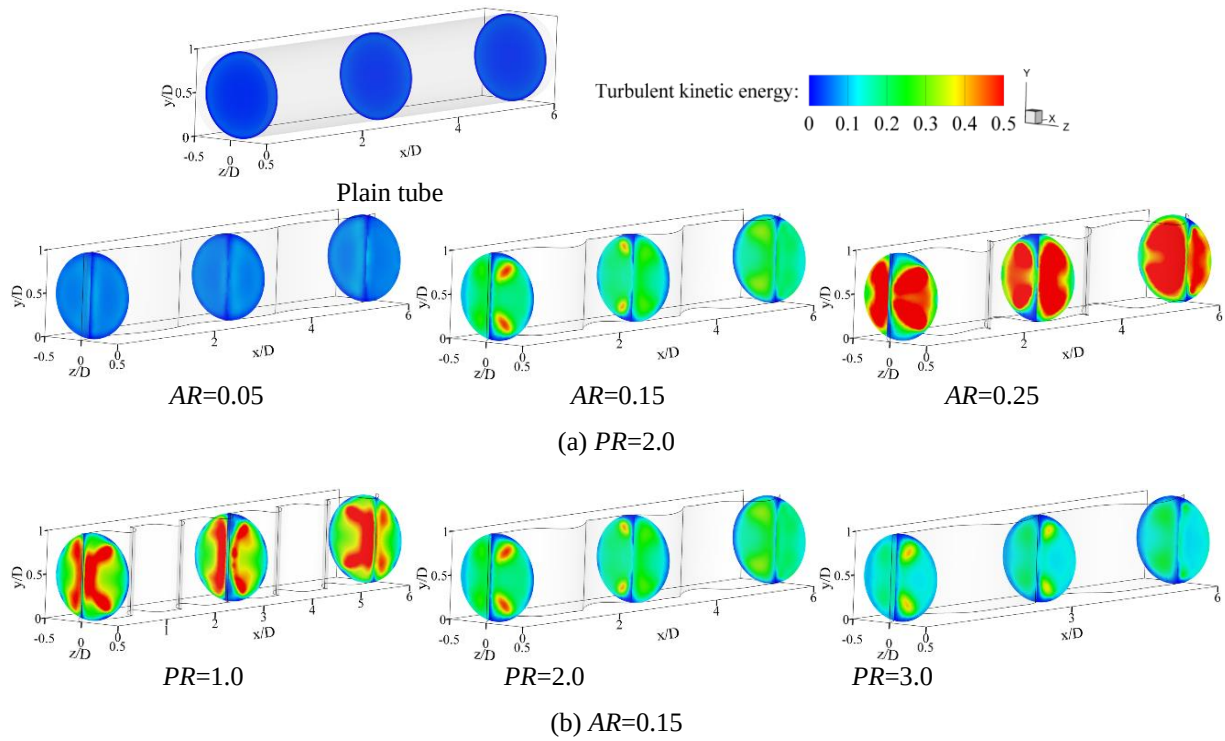

Fig. 7. TKE distribution for (a) effect of *AR* and (b) effect of *PR* at *Re* = 5000.

4.4 Heat transfer mechanism

The heat transfer characteristics of the tube equipped with sinusoidal baffles are represented by the fluid temperature distribution over the cross–sectional plane and the local wall Nusselt number as shown in Fig. 8 and 9, respectively. The effect of the sinusoidal baffles in the tube demonstrates the influence of *AR* and *PR* compared to that of a plain tube at the same *Re* = 5000.

Figures 8a and b display the fluid temperature distribution in the cross–sectional plane showing the effect of varying *AR* and *PR*, respectively. In general, a plain tube exhibits a high fluid temperature (larger thermal boundary layer) near the tube wall while low fluid temperature appears at the core. This thermal boundary layer blocks heat transfer between the heated tube wall and the fluid. Using sinusoidal baffles, the thermal boundary layer is thinner due to greater fluid velocity. Additionally, low temperature fluid is forced to a near-wall position due to the reattachment of flow, leading to increased heat transfer between the heated tube wall and the fluid. As the *AR* is increased, the thermal boundary layer becomes thinner due to stronger flow, especially at *AR* = 0.25. This condition provides the thinnest thermal boundary layer compared to other *AR*s. Increasing the *PR* value led to increased thermal boundary layer thickness due to decreased flow strength. *PR* = 3.0 provided the thickest thermal boundary layer.

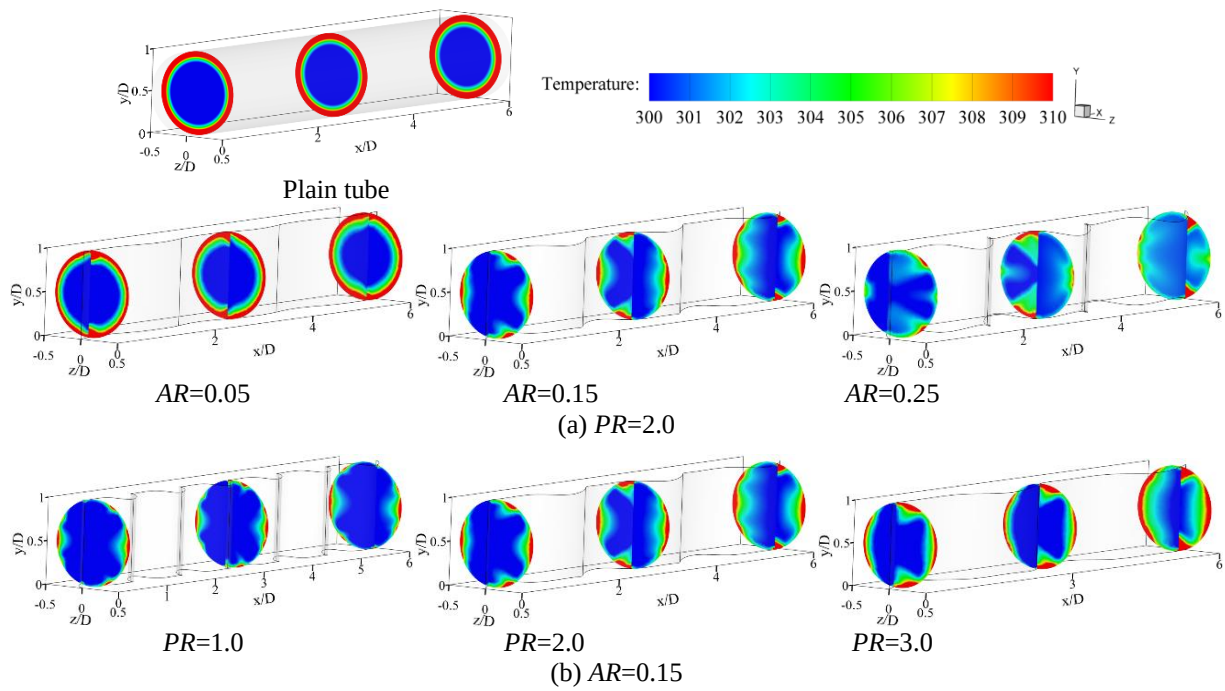

Fig. 8. Temperature distribution for (a) effect of *AR* and (b) effect of *PR* at *Re* = 5000.

Figures 9a and b show local heat transfer at the tube wall in the form of the local wall Nusselt number for the effects of *AR* and *PR*, respectively. In the figure, the tube equipped with sinusoidal baffles provided greater heat transfer at the tube wall than the plain tube. Optimal heat transfer was detected at the upper–lower regions, in which disruption of the thermal boundary layer was greatest due to the strength of the flow. *AR* = 0.25 provided the highest heat transfer of all *AR* values due to thermal boundary layer disruption, while *PR* = 3.0 showed the lowest heat transfer due to the greater thickness of the thermal boundary layer.

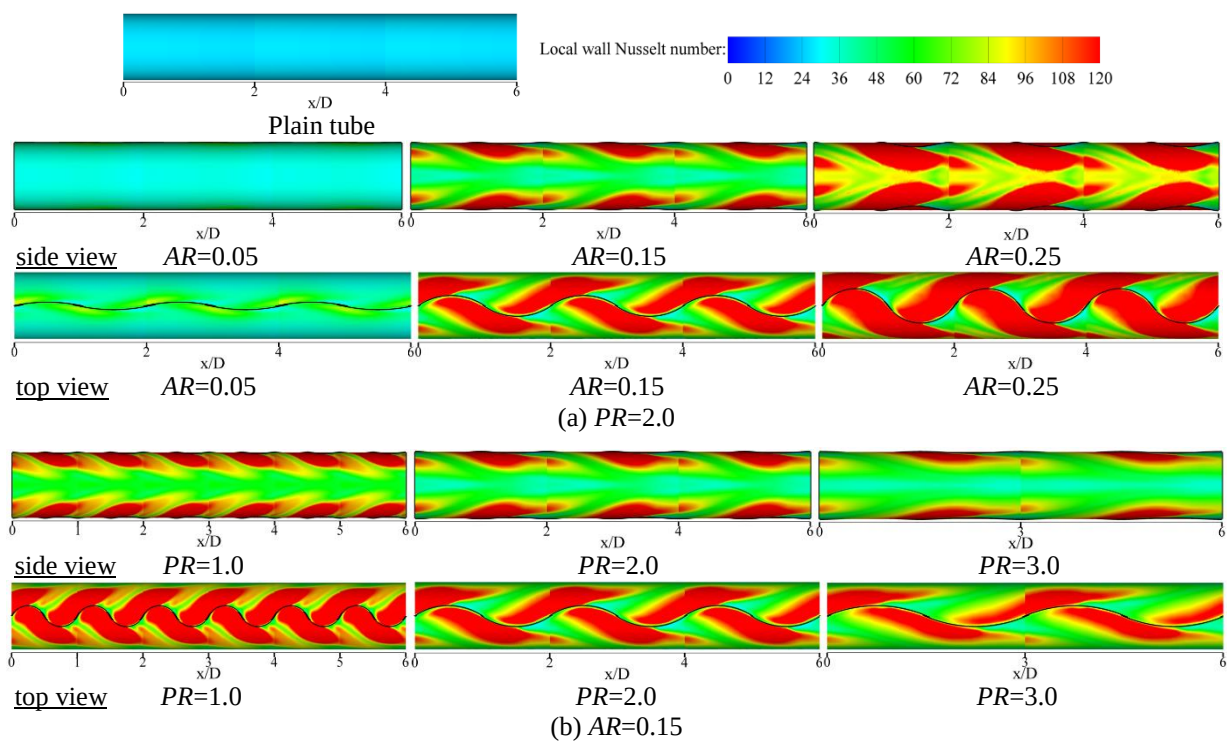

Fig. 9. Local wall Nusselt number for (a) effect of *AR* and (b) effect of *PR* at *Re* = 5000.

5. PERFORMANCE ASSESSMENT

The dimensionless parameters in the current study, the Nusselt number (Nu), Nusselt number ratio (Nu/Nu_0), friction factor (f), friction factor ratio (f/f_0) and thermal enhancement factor (TEF) were used to analyze the thermal performance of a circular tube heat exchanger equipped with sinusoidal baffles. The effects of Re, AR and PR are presented below.

5.1 Effect of Re

Figures 10a, b, c, and d present the relationships of Nu, Nu/Nu_0, f, f/f_0 and TEF with Re, respectively. Generally, the inclusion of sinusoidal baffles in a tube heat exchanger can increase heat transfer ($Nu/Nu_0 > 1$). The Nu increased with Re due to increased fluid velocity leading greater flow intensity at the tube wall. Conditions where Re = 20,000 promoted the strongest flow, which greatly disrupted the thermal boundary layer. The heat transfer ratio, Nu/Nu_0, decreased with increasing Re values. The Nusselt number was found to be in the range 48.74–375.26 or 125.28-539.61% and 1.73–7.78 times greater than the plain tube in terms of Nu/Nu_0 values for Re = 5000–20,000.

The tube equipped with sinusoidal baffles not only showed increased heat transfer, but a greater pressure drop due to the flow blockage. In general, the inclusion of sinusoidal baffles in the tube resulted in higher friction factors ($f/f_0 > 1$). The f and f/f_0 values decreased with increasing Re all cases, because the shear stress of the fluid was reduced. The f and f/f_0 values ranged from 0.1–5.22 and 3.6–117.06 times greater, respectively, over the plain tube for Re = 5000–20,000.

The overall thermal performance of the tube equipped with sinusoidal baffles is presented in terms of the thermal enhancement factor (TEF). For all cases investigated, the TEF of tubes equipped with sinusoidal baffles was higher than that of the plain tube ($TEF > 1$) for Re = 5000–20,000. The TEF decreased with increasing Re, and was found to be approximately 1.12–1.89 times higher or 12–89% greater than the plain tube.

5.2 Effect of AR and *PR*

The relationships of the Nu/Nu_0, f/f_0 and TEF with AR at various PR values are depicted in Figs. 11a, b and c, respectively, for Re = 5000, 10000, 16000 and 20000. The results in Fig. 11a reveal that incremental increases in AR led to increased heat transfer because of greater flow intensity. Alternatively, an increased PR value led to decreased heat transfer due to a decay in flow intensity. The maximum Nu/Nu_0 was found at AR = 0.25, PR = 1.0 and Re = 5000 while the minimum Nu/Nu_0 was found at AR = 0.05, PR = 3.0 and Re = 20,000. For all AR values, Nu/Nu_0 was found to be 2.07–7.78, 1.85–6.01 and 1.77–5.04 times higher, respectively, for PR = 1.0, 2.0 and 3.0.

The effect of AR and PR on the pressure drop in terms of the f/f_0 value is depicted in Fig. 11b. In this figure, increasing the AR value resulted in increased f/f_0 due to decreased area available for flow while an incremental increase in PR led to a decreased f/f_0. The greatest f/f_0 was found in the range, $0.15 \leq AR \leq 0.25$, for all PR values. For all AR, values, the f/f_0 values were in the range of 4.2–117.06, 3.9–46.65 and 3.6–30.52 times higher than plain tube, respectively, for PR = 1.0, 2.0 and 3.0.

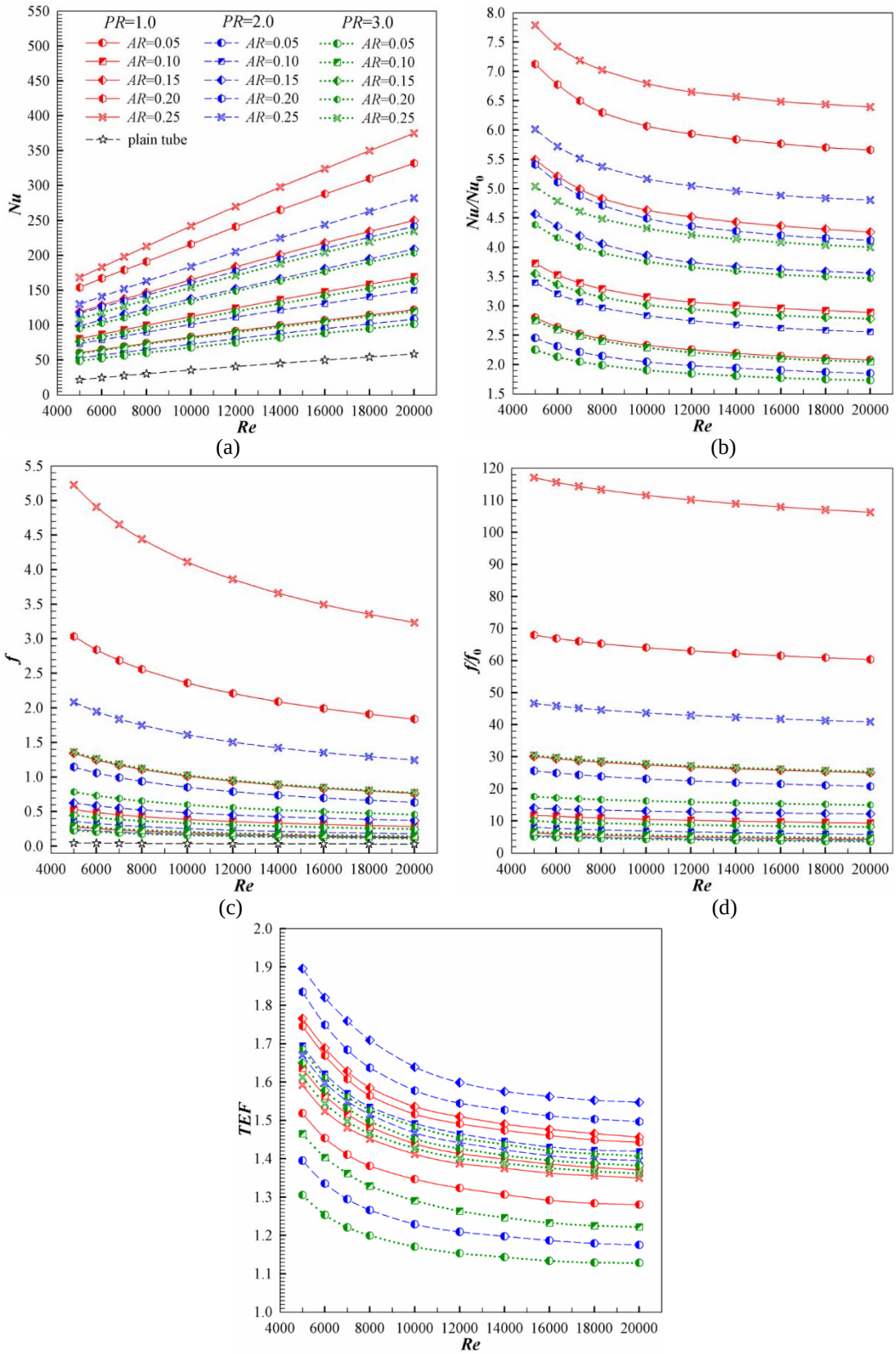

Fig. 10. The relationships of (a) Nu, (b) Nu/Nu_0, (c) f, (d) f/f_0 and (e) TEF with Re.

Figure 11c shows the relationship of the *TEF* with *AR* at various *PR* values. In the figure, it can be seen that the tube equipped with sinusoidal baffles at *AR* = 0.15 and *PR* = 2.0 gave the highest *TEF*. The maximum *TEF* was found to be 1.89 at *Re* = 5000. For *PR* = 1.0, 2.0 and 3.0. The maximal *TEF* was detected at *AR* = 0.15, 0.15 and 0.20, respectively. This indicates that the optimum *TEF* appeared at *AR* = 0.15–0.20. For all *AR* values, the *TEF* was found to range from 1.28–1.76, 1.17–1.89 and 1.12–1.68, respectively, for *PR* = 1.0, 2.0 and 3.0.

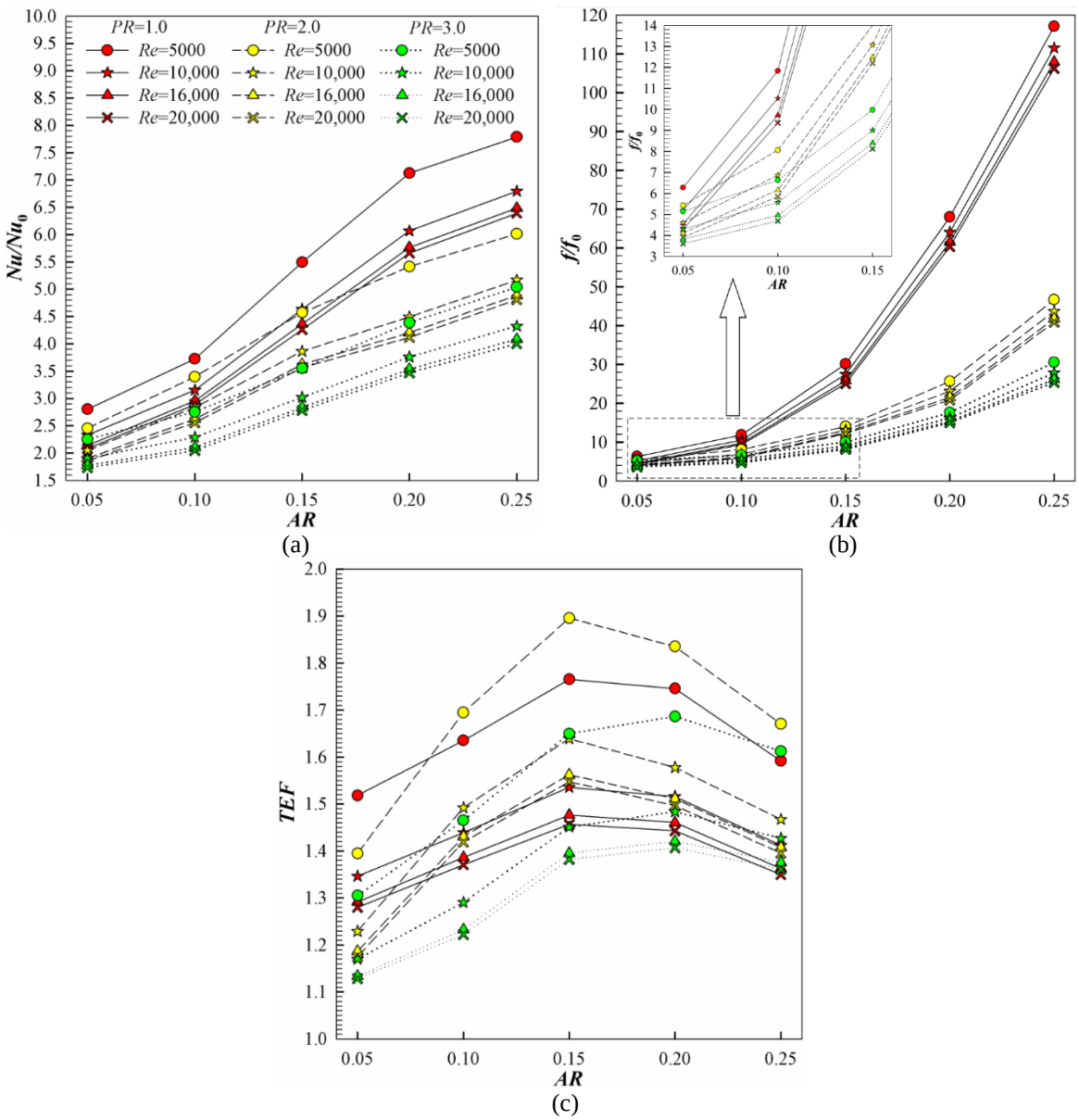

Fig. 11. The relationship of (a) Nu/Nu_0, (b) f/f_0 and (c) *TEF* with *AR* at various *PR* values.

6. COMPARISON OF PUBLISHED RESULTS FOR CIRCULAR TUBE INSERTS

The maximum *TEF* using sinusoidal baffle inserts in the present work is compared with the values for other baffle inserts found in the literature [3–14] and is presented in Fig. 12. The maximum *TEF* for each study was selected for comparison. Determination of the *TEF* using Eq. (14) at a constant pumping power showed a decreasing *TEF* with increasing *Re*. In the figure, the *TEF* range from 0.82 to 1.9 depending on the baffle geometry. The sinusoidal baffles provided an average *TEF* that was higher than that of other baffle inserts by approximately 9.17–70.86%, but was still 3.42% less than the baffle insert of Skullong et al. [8].

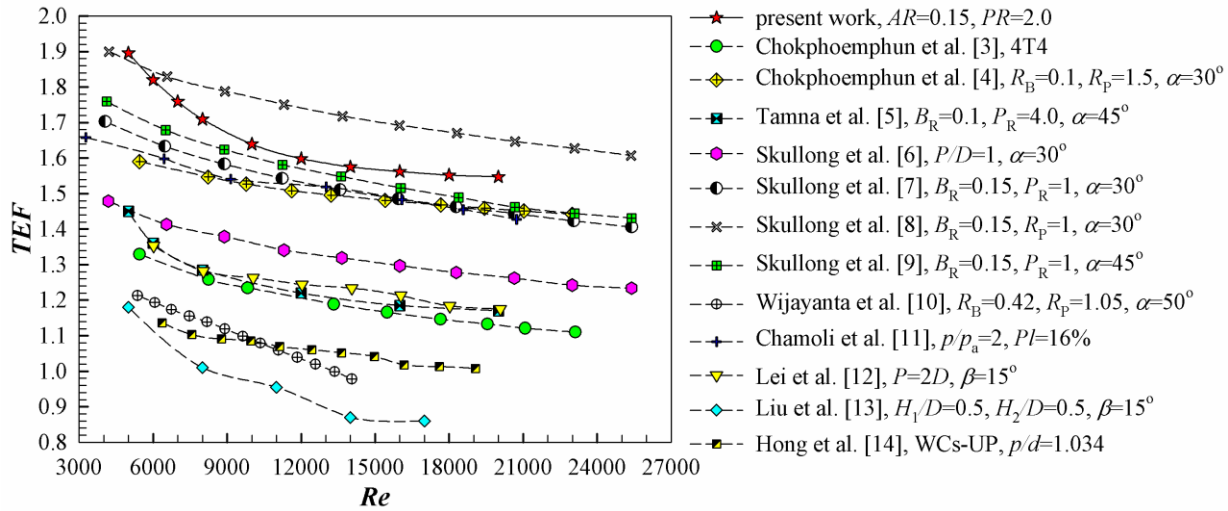

Fig. 12. Comparison of published *TEF* values using circular tube inserts.

7. CONCLUSIONS

The flow structure and heat transfer characteristics of a circular tube equipped with sinusoidal baffles at *AR* = 0.05, 0.10, 0.15, 0.20, 0.25 and *PR* = 1.0, 2.0, 3.0 with *Re* ranging from 5000–20,000 with a heated wall are reported based on a numerical investigation of turbulent flow and heat transfer characteristics. Heat transfer, friction factors and thermal enhancement factors were considered. As a result, the sinusoidal baffles generated reattachment flow at the tube wall leading to disruption of the thermal boundary layer near the tube wall and subsequent increased heat transfer and thermal enhancement factors. Increasing the heat transfer rate depends on the intensity of flow near the tube wall. This was determined by increasing *Re* and *AR* and decreasing *PR*. Sinusoidal baffles considerably increase heat transfer and the friction factor, with *Nu* = 48.74–375.26 and *f* =0.1–5.22, respectively, above that of a plain tube. Comparison with a plain tube yielded values of the Nu/Nu_0 and the f/f_0 1.73–7.78 and 3.6–117 times higher, respectively. The response depends on the *Re*, *AR* and *PR* values. The *TEF* was found to be about 1.12–1.9 times higher than plain tube, over the range of values investigated. *PR* = 2.0 and *AR* = 0.20 provided a maximal *TFE* of 1.9 at *Re* = 5000. The best operating regime in all cases was found at the lowest *Re* values.

NOMENCLATURE

A	heat transfer area, m^2
AR	amplitude ratio
C_1	turbulent model coefficient, dimensionless
C_2, $C_{1\varepsilon}$	turbulent model constant, dimensionless
$C_{3\varepsilon}$	degree of ε by the buoyancy, dimensionless
c_p	specific heat, J kg^{-1} K^{-1}
D	tube diameter, m
D_h	hydraulic diameter, m
E	total energy, J/kg
e	sinusoidal baffle amplitude, m
f	friction factor, dimensionless
G_b	production of turbulence kinetic energy due to buoyancy, kg s^{-3}
G_k	production of turbulent kinetic energy due to the mean velocity gradient, kg s^{-3} m^{-1}
h	convective heat transfer coefficient, W m^{-2} K^{-1}
h_x	local convective heat transfer coefficient, W m^{-2} K^{-1}
k	turbulent kinetic energy, m^2 s^{-2}
k_a	thermal conductivity of air, W m^{-1} K^{-1}
Nu	average Nusselt number, dimensionless
Nu_x	local Nusselt number, dimensionless

Pr	Prandtl number, dimensionless
PR	pitch ratio, dimensionless
p	sinusoidal baffle pitch, m
P	pressure, Pa
Re	Reynolds number, dimensionless
S	magnitude of mean strain rate, s^{-1}
S_{ij}	mean strain rate tensor, s^{-1}
S_k	user–defined source term for k, kg m^{-1} s^{-3}
S_ε	user–defined source term for ε, kg m^{-1} s^{-4}
T	temperature, K
TEF	thermal enhancement factor, dimensionless
U	mean velocity, m s^{-1}
u_i	velocity component in x_i–direction, m s^{-1}
u_i'	fluctuation velocity in x_i–direction, m s^{-1}
u_j	velocity component in x_j–direction, m s^{-1}
u_j'	fluctuation velocity in x_j–direction, m s^{-1}
u_k	velocity component in x_k–direction, m s^{-1}
x	x–position, m
y	y–position, m or distance from the wall, m
z	z–position, m

Greek letters

μ	dynamic viscosity, kg s^{-1} m^{-1}
σ_k	turbulent Prandtl numbers for k, dimensionless
σ_ε	turbulent Prandtl numbers for ε, dimensionless
δ_{ij}	Kronecker delta, m
ε	turbulent dissipation rate, m^2 s^{-3}
ρ	density, kg m^{-3}
η	ratio of the turbulent to mean strain, dimensionless
ν	kinematic viscosity, m^2 s^{-1}
τ_0	shear stress at the wall, N m^{-2}
τ_{eff}	deviatoric stress tensor

Subscripts

0	plain tube
a	air
t	turbulent
i, j, k	directions of the coordinate system

Superscripts

—	average

REFERENCES

[1] Deshmukh, P.W. and Vedula, R.P. Heat transfer and friction factor characteristics of turbulent flow through a circular tube fitted with vortex generator inserts, Int. J. Heat Mass Transfer, Vol. 79, 2014, pp. 551-560.

[2] Deshmukh, P.W., Prabhu, S.V. and Vedula, R.P. Heat transfer enhancement for laminar flow in tubes using curved delta wing vortex generator inserts, Appl. Therm. Eng., Vol. 106, 2016, pp. 1415-1426.

[3] Chokphoemphun, S., Pimsarn, M., Thianpong, C. and Promvonge, P. Thermal performance of tubular heat exchanger with multiple twisted–tape inserts, Chin. J. Chem. Eng., Vol. 23, 2015, pp. 755-762.

[4] Chokphoemphun, S., Pimsarn, M., Thianpong, C. and Promvonge, P. Heat transfer augmentation in a circular tube with winglet vortex generators, Chin. J. Chem. Eng., Vol. 23, 2015, pp. 605-614.

[5] Tamna, S., Sripattanapipat, S. and Promvonge, P. Numerical heat transfer study of turbulent tube flow through winglet–pairs, Energy Procedia, Vol. 100, 2016, pp. 518-521.
[6] Skullong, S., Promvonge, P., Jayranaiwachira, N. and Thianpong, C. Experimental and numerical heat transfer investigation in a tubular heat exchanger with delta–wing tape inserts, Chem. Eng. Process. Process Intensif., Vol. 109, 2016, pp. 164-177.
[7] Skullong, S., Promvonge, P., Thianpong, C. and Pimsarn, M. Heat transfer and turbulent flow friction in a round tube with staggered–winglet perforated–tapes, Int. J. Heat Mass Transfer, Vol. 95, 2016, pp. 230-242.
[8] Skullong, S., Promvonge, P., Thianpong, C. and Jayranaiwachira, N. Thermal behaviors in a round tube equipped with quadruple perforated–delta–winglet pairs, Appl. Therm. Eng., Vol. 115, 2017, pp. 229-243.
[9] Skullong, S., Promvonge, P., Thianpong, C., Jayranaiwachira, N. and Pimsarn, M. Thermal performance of heat exchanger tube inserted with curved winglet tapes, Appl. Therm. Eng., Vol. 129, 2018, pp. 1197-1211.
[10] Wijayanta, A.T., Istanto, T., Kariya, K. and Miyara, A. Heat transfer enhancement of internal flow by inserting punched delta winglet vortex generators with various attack angles, Exp. Therm. Fluid Sci., Vol. 87, 2017, pp. 141-148.
[11] Chamoli, S., Lu, R. and Yu, P. Thermal characteristic of a turbulent flow through a circular tube fitted with perforated vortex generator inserts, Appl. Therm. Eng., Vol. 121, 2017, pp. 1117-1134.
[12] Lei, Y., Zheng, F., Song, C. and Lyu, Y. Improving the thermal hydraulic performance of a circular tube by using punched delta–winglet vortex generators, Int. J. Heat Mass Transfer, Vol. 111, 2017, pp. 299-311.
[13] Liu, H.L., Li, H., He, Y.L. and Chen, Z.T. Heat transfer and flow characteristics in a circular tube fitted with rectangular winglet vortex generators, Int. J. Heat Mass Transfer, Vol. 126, 2018, pp. 989-1006.
[14] Hong, Y., Du, J., Wang, S., Huang, S.M. and Ye, W.B. Heat transfer and fluid flow behaviors in a tube with modified wire coils, Int. J. Heat Mass Transfer, Vol. 124, 2018, pp. 1347-1360.
[15] Promthaisong, P., Kumar, M., Chuwattanakul, V., Saysroy, A. and Eiamsa-ard, S. Prediction of heat and fluid flow in a heat exchanger tube mounted with V-cone bundles, J. Res. Appl. Mech. Eng., Vol. 6(1), 2018, pp. 13-20.
[16] Patankar, S.V. Numerical heat transfer and fluid flow, 1980, McGraw–Hill, New York.
[17] Kumar, A., Maithani, R. and Suri, A.R.S. Numerical and experimental investigation of enhancement of heat transfer in dimpled rib heat exchanger tube, Heat Mass Transfer., Vol. 53, 2017, pp. 3501-3516.
[18] Incropera, F.P., Witt, P.D., Bergman, T.L. and Lavine, A.S. Fundamentals of heat and mass transfer, 2006, John Wiley & Sons, New York.
[19] Suwannapan, S., Skullong, S. and Promvonge, P. Thermal characteristics in a heat exchanger tube fitted with zigzag-winglet perforated-tapes, J. Res. Appl. Mech. Eng., Vol. 3(1), 2015, pp. 29-36.
[20] Sripattanapipat, S., Tamna, S., Jayranaiwachira, N. and Promvonge, P. Numerical heat transfer investigation in a heat exchanger tube with hexagonal conical-ring inserts, Energy Procedia, Vol. 100, 2016, pp. 522-525.
[21] Cheng, J., Qian, Z. and Wang, Q. Analysis of heat transfer and flow resistance of twisted oval tube in low Reynolds number flow, Int. J. Heat Mass Transfer, Vol. 109, 2017, pp. 761-777.
[22] Promthaisong, P., Jedsadaratanachai, W. and Eiamsa-ard, S. 3D Numerical study on the flow topology and heat transfer characteristics of turbulent forced convection in spirally corrugated tube, Numer. Heat Transfer A., Vol. 69(6), 2016, pp. 607-629.